# A Study of Planetary Waves in the Southern Winter Troposphere and Stratosphere. Part I: Wave Structure and Vertical Propagation

WILLIAM J. RANDEL

*National Center for Atmospheric Research,* Boulder, CO 80307*

(Manuscript received 2 January 1986, in final form 25 August 1986)

ABSTRACT

Planetary wave propagation in the southern winter troposphere and stratosphere is studied in an attempt to trace the origins of upward propagating disturbance. Daily geopotential grids from 1000 to 1 mb are analyzed for two 120-day winter seasons. A cross-correlation analysis technique is developed which allows coherent wave structure to be traced in time. Significant correlations are observed between the troposphere and stratosphere at finite time lags, indicative of vertically propagating waves. The observed vertical propagation time scales between the middle troposphere and middle stratosphere are on the order of 4 days for zonal wavenumber 1 ($k = 1$), 1–2 days for $k = 2$, and 1 day for $k = 3$.

The cross-correlation analysis also delineates the meridional and vertical structures of the transient (in time) planetary waves. Zonal wavenumber 1 fluctuations exhibit a vertical out-of-phase relationship between the midlatitude troposphere and stratosphere. Three out-of-phase maxima in latitude are observed in the troposphere, separated by 25–30° latitude, whereas a single broad latitudinal maximum is found in the stratosphere. Wavenumbers 2 and 3 exhibit similar overall structures, quite distinct from that of $k = 1$. Two out-of-phase maxima in latitude are observed in the troposphere, separated by 30–35° latitude, and the stratospheric variance is found to be coherent and in phase with that in the high latitude troposphere.

## 1. Introduction

There is considerable evidence that the intermittent appearance of amplified planetary scale disturbances in the winter stratosphere is linked to the upward propagation of wave activity from lower levels. Numerous observational studies such as Muench (1965), Hirota and Sato (1969), O'Neill and Taylor (1979), and Quiroz (1979), have convincingly shown that planetary waves propagate from the troposphere into the stratosphere during winter in the Northern Hemisphere (NH). The objective of this study is to analyze this phenomenon during winter in the Southern Hemisphere (SH); we hope to trace the sources of stratospheric planetary waves into the troposphere and learn something of their origins there. The choice here of studying the SH is based primarily on the fact that forced stationary waves in the SH are of much smaller amplitude than their northern counterparts (van Loon and Jenne, 1972); the majority of wave activity in the southern winter stratosphere is contained in transient and traveling waves. If one hopes to isolate important aspects of transient vertically propagating waves, the SH may afford a "cleaner" environment than the NH. In addition, the zonal wavenumber 2 component in the SH often exhibits regular eastward propagation, whereas the wavenumber 1 component is quasi-stationary (Harwood, 1975; Hartmann, 1976; Leovy and Webster, 1976). In contrast, both are quasi-stationary in the NH (Leovy and Webster, 1976). This zonal dispersion suggests a degree of independence between zonal wavenumber $k = 1$ and 2 in the SH; we wish to further explore this behavior.

In a recent observational study Mechoso and Hartman (1982) tried to trace the origins of SH stratospheric planetary waves, based on space-time cross-spectral analysis. To their surprise they found the eastward moving stratospheric variance to be linearly independent of that in the troposphere. They suggested that this linear incoherence could result from (i) finite travel time between the troposphere and stratosphere, (ii) in situ instabilities, and/or (iii) the presence of two independent linear modes.

The present study (Part I) is based on a cross-correlation analysis technique that can incorporate time lag information. We find significant coherence between the troposphere and stratosphere at finite time lags, indicating that the stratospheric maxima can be traced into the troposphere if the finite transit time is taken into account; this confirms the above hypothesis (i) of Mechoso and Hartmann (1982). In addition, the cross-correlation analysis developed here delineates the wave structure in the meridional plane, revealing remarkable coherent in and out of phase fluctuations throughout the troposphere and stratosphere.

Part II of this study (Randel et al., 1987) is an analysis of the observed life-cycles of the vertically propagating planetary waves, based on wave–mean flow interaction diagnostics. Two important results from Part II are particularly relevant to Part I: 1) planetary wave energetics in the stratosphere can be understood quantitatively in terms of upward propagation from the troposphere, discounting in situ stratospheric planetary wave energy sources, and 2) although stratospheric events can be clearly traced into the troposphere, not

* The National Center for Atmospheric Research is sponsored by the National Science Foundation.

all tropospheric planetary waves propagate into the stratosphere (see Fig. 13 of Part II). This factor causes the linear correlation between these regions to be reduced, although it is still large enough to be statistically significant.

## 2. Data and analysis technique

### *a. Data*

The data used in this study are gridded geopotential heights from 1000 to 0.4 mb archived at the National Center for Atmospheric Research. Grids below 100 mb are the 12Z NMC analyses, while data from 70 to 0.4 mb are satellite-derived geopotential thicknesses (produced at the Climate Analysis Center, Washington, DC) stacked on top of the 100 mb NMC grids. Because the 0.4 mb level lies substantially above the peak of the highest satellite radiometer weighting function (SSU channel 3, which peaks near 1–2 mb), the data at this level are of suspect quality and not used in this study. The grids were harmonically analyzed on constant latitude circles to allow analyses based on zonal wavenumber.

Data for two 120-day winter seasons (1 June–28 September 1983 and 1984) were analyzed. Because of the nature of the database and the uncertainties involved, the results from the two winters were compared for consistent behavior. Despite the complexity of the coherent wave fluctuations observed here, a high degree of consistency is observed between the two winters, suggesting that these observations represent fundamental atmospheric behavior. To minimize space, analyses of one winter (1983) are primarily discussed here.

### *b. Analysis technique*

#### 1) MOTIVATION–EPISODIC BEHAVIOR OF PLANETARY WAVES

The dominance of planetary-scale waves in the winter stratosphere is well-documented observationally. Figure 1 shows this behavior during the 1983 SH winter. Here the average amplitude of the transient wave geopotential height fluctuations and average transient EP flux diagrams for zonal wavenumbers 1 through 4 are displayed, demonstrating the distinctive character-

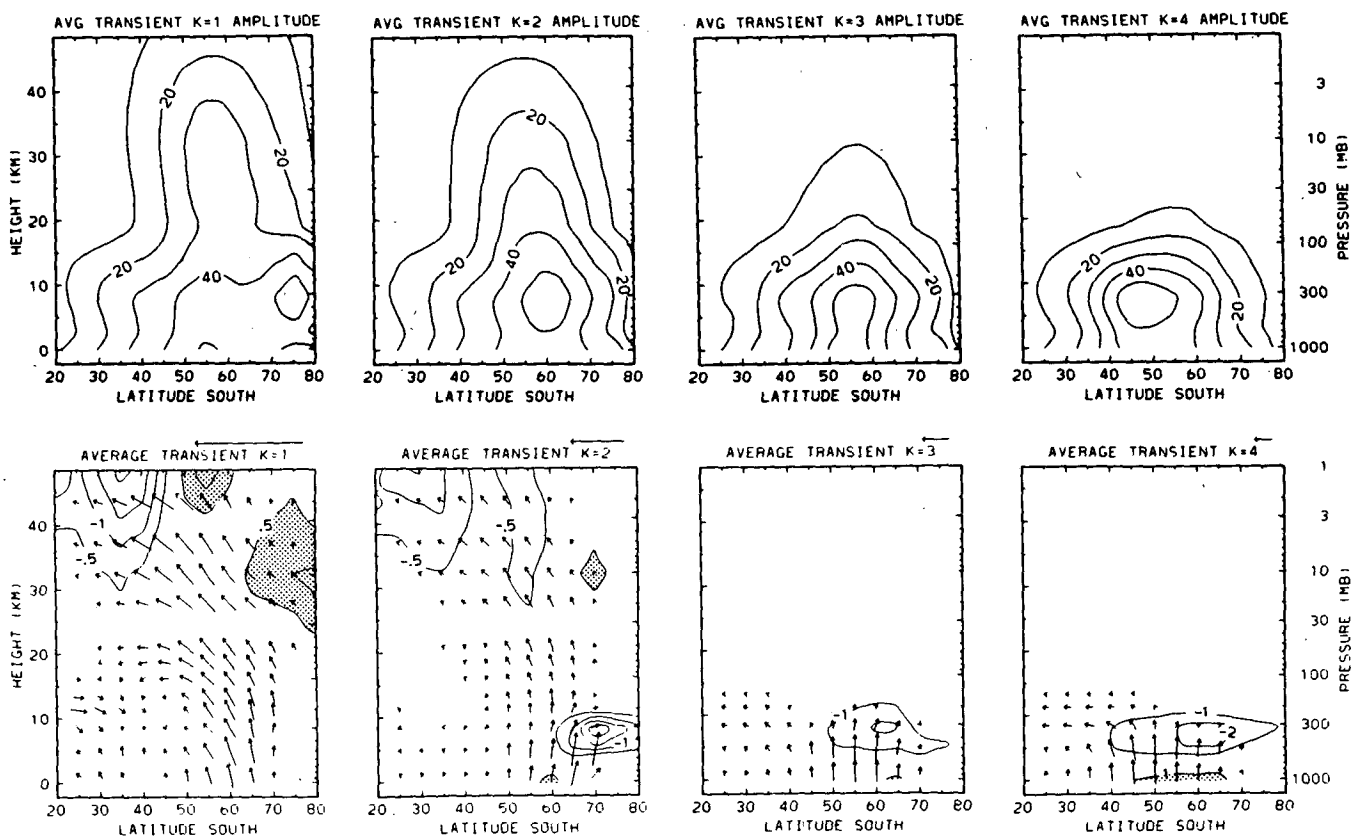


FIG. 1. Average amplitude of transient geopotential height fluctuations scaled by inverse square root of density (top-units of gpm) and time-averaged EP flux diagrams (bottom) for zonal wavenumbers 1 through 4 individually during 1 June–28 September 1983. Calculation of the EP flux diagnostics are discussed in Part II. The reference arrow scale in the top right corner of each plot denote 15 $m^2 s^{-2}$ of $F_\phi$ and 0.1 $m^2 s^{-2}$ of $F_Z$, while the contours are of the EP flux divergence (contour intervals of 0.5 m $s^{-1}$ per day for $k = 1$ and $k = 2$, and 1.0 m $s^{-1}$ per day for $k = 3$ and $k = 4$).

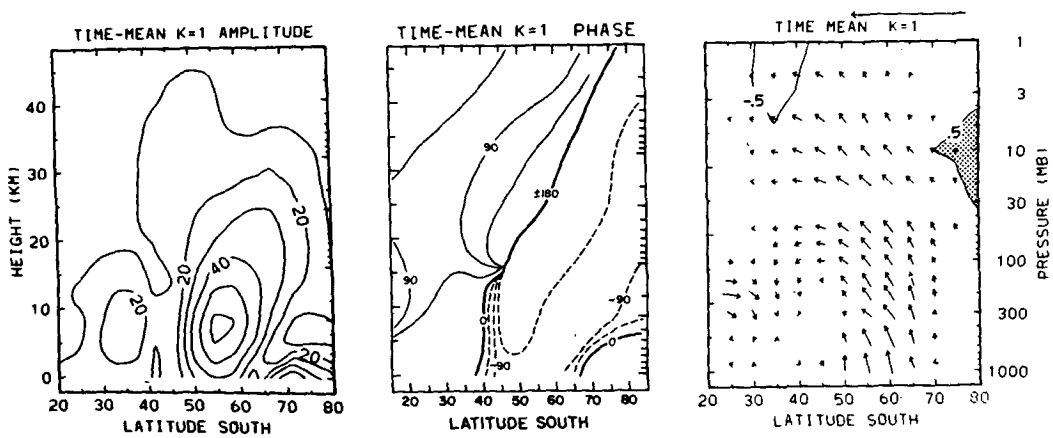


FIG. 2. Amplitude scaled by inverse square root of density (left-units of gpm), phase (center-longitude of ridge), and EP flux diagram (right, contours of 0.5 m $s^{-1}$ per day) for the time-mean wave 1 component during the period 1 June–28 September 1983.

istics of the different transient wave scales. "Average transient" is defined here to be the time average of the daily values, with the seasonal (120-day) mean removed. The wave amplitudes are weighted by $e^{-Z/2H}$ to remove the effect of density stratification. The EP flux diagrams are based on the quasi-geostrophically scaled equations, using the wind fields discussed in Part II.

Figure 1 shows that waves 1 and 2 contribute the dominant transient geopotential height variance above 100 mb; wave 3 contributes a small amount in the stratosphere. The EP flux signatures show the $k$ = 1–

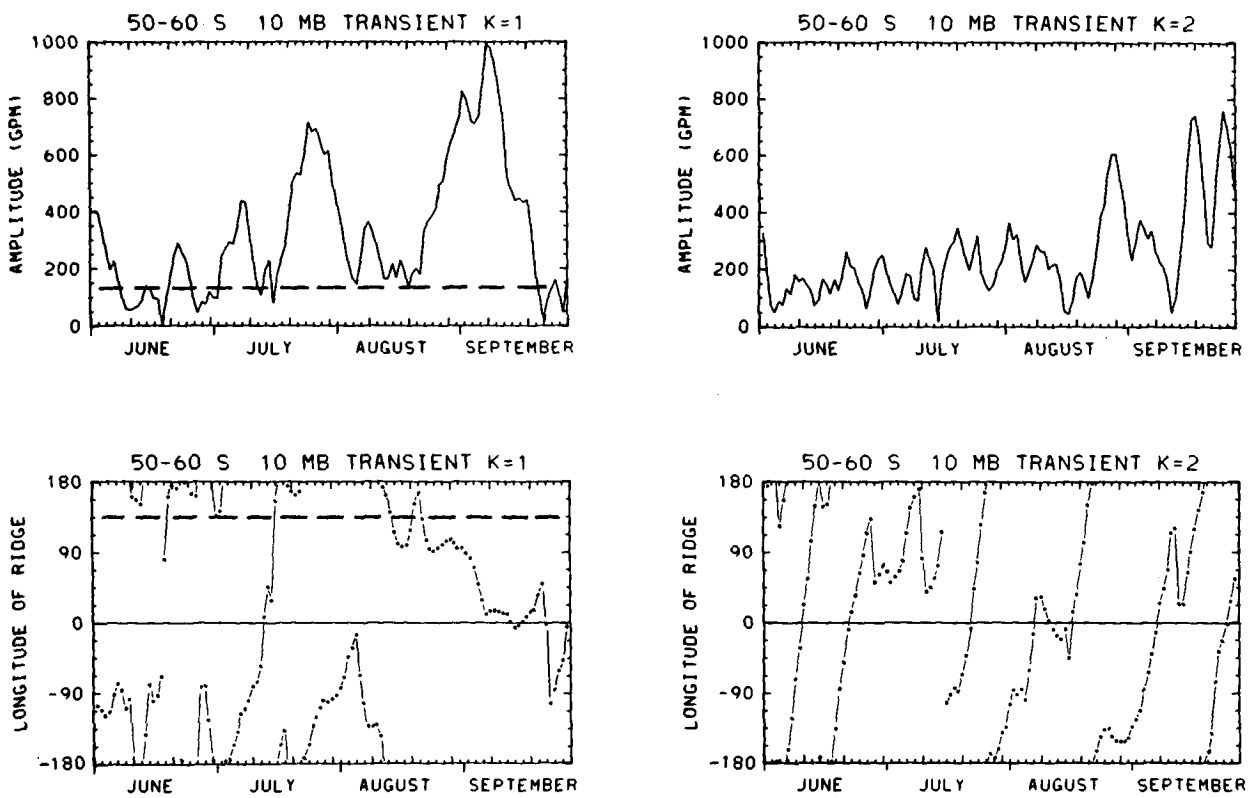


FIG. 3. Amplitude (gpm) and phase (longitude of ridge) of zonal wavenumber 1 and 2 *transient* fluctuations at 10 mb, averaged over 50–60°S. Additionally, the time mean values for wave 1 are indicated by the dashed lines. Note the regular eastward progression of wave 2.

2 dominance in the stratosphere as well; similar results were observed during the SH winter of 1979 by Hartmann et al. (1984). Zonal wavenumber 4 (and higher) are clearly tropospheric modes; their EP flux signatures are indicative of baroclinic wave life cycles (Edmon et al., 1980, Randel and Stanford, 1985). The midlatitude baroclinic activity during this season shows a clear spectral peak at zonal wavenumber 4, whereas significant low latitude contributions are spread over the wave band $k$ = 4–7. Figure 1 suggests that wave 3 also contributes much of the high latitude baroclinic wave variance. Figure 2 shows the geopotential height amplitude and phase, and EP flux diagram for the time-mean (120-day) wave 1 component; higher wavenumber contributions are small. Comparison between Figs. 1 and 2 shows that the stationary component is much smaller than the average transient waves during this year. This situation is quite distinct from that in the NH, where the stationary wave amplitudes are comparable to or larger than the average transient.

Time series of the amplitudes and phases of transient waves 1 and 2 at 10 mb averaged over 50°–60°S are shown in Fig. 3; in addition, the time-mean wave 1 component is indicated by the superimposed dashed lines. Note that the large wave 1 amplitude fluctuations are not well correlated with the phase of the wave, as would result from stationary–transient interference. The amplitude of transient wave 1 fluctuates irregularly with a time scale on the order of 20 days; the phase is highly variable or slowly westward moving over much of the winter. Wave 2 amplitude also exhibits episodic behavior, but the phase is often found to move regularly eastward with a period near 10–15 days.

Inspection of the amplitudes and phases of waves 1 and 2 reveals little correlation between wave amplitude and either phase position or regular phase movement. Rather, the growth of wave amplitude appears to occur in episodic events, presumably the result of episodic tropospheric forcing. In this study we analyze coherent variations throughout the troposphere and stratosphere

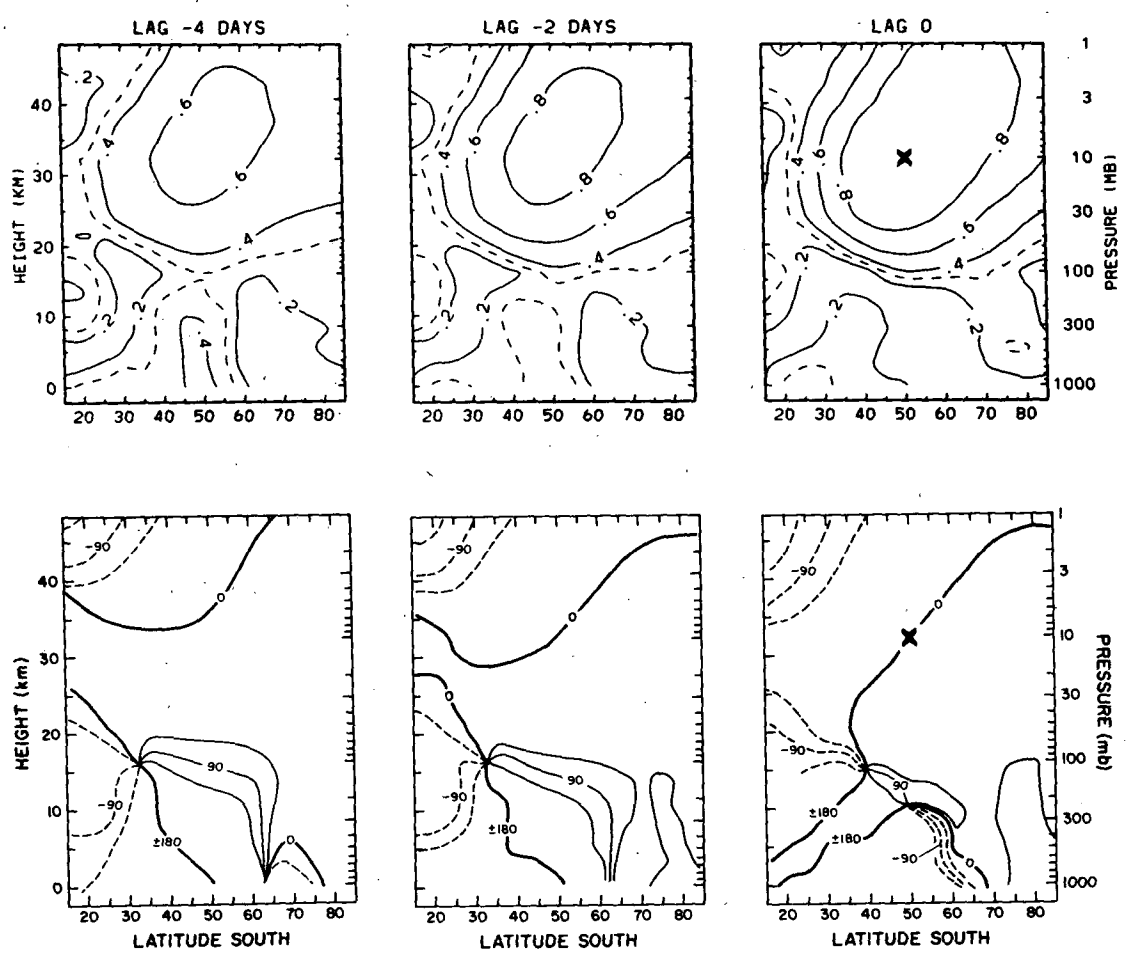


FIG. 4. Correlation coherence (top) and phase (bottom) for wave 1 geopotential height fluctuations with respect to 10 mb, 50°S and zero time lag, for time lags of −4 (left), −2 (middle), and 0 days (right). Contour interval of coherence is 0.2, with the 0.3 contour added as a dashed line. Phase is measured in degrees longitude relative to the reference position (positive is eastward). In this and the following figures the reference position is marked with an 'X' on the lag 0 plot.

via cross-correlation analyses, allowing time lag information to be incorporated in the hope of tracing wave evolution.

2) CROSS-SPECTRAL CORRELATION ANALYSIS

We wish to consider the cross-correlation between zonal Fourier coefficients of wavenumber $k$ at two different latitudes and pressures [$Z1$ is at $(\phi_1, P_1)$ and $Z2$ at $(\phi_2, P_2)$]:

$$Z1_k(x,t) = S1_k(t) \cdot \sin(kx) + C1_k(t) \cdot \cos(kx)$$

$$Z2_k(x,t) = S2_k(t) \cdot \sin(kx) + C2_k(t) \cdot \cos(kx).$$

Hereafter, the subscript $k$ will be understood. By analogy with cross-spectral analysis we define the *in-phase* correlation between $Z1(x, t)$ and $Z2(x, t)$ as

$$CO_\tau = \langle S1, S2\rangle_\tau + \langle C1, C2\rangle_\tau \qquad (1a)$$

where

$$\langle S1, S2\rangle_\tau = \frac{\frac{1}{N-\tau}\sum_{t=1}^{N-Z} S1(t) \cdot S2(t+\tau)}{\sigma_{Z1} \cdot \sigma_{Z2}}$$

measures the linear correlation at time lag $\tau$ between $S1(t)$ and $S2(t)$ (the time mean values have been removed), and $\sigma_{Z1}(\sigma_{Z2})$ is the square root of the variance of $Z1(x, t)(Z2(x, t))$, i.e.

$$\sigma_{Z1} = \left(\frac{1}{N-1}\sum_{t=1}^{N} (S1(t)^2 + C1(t)^2)\right)^{1/2},$$

$\langle C1, C2\rangle_\tau$ is given by a similar expression. The *out-of-phase* correlation is given by

$$QD_\tau = \langle S1, C2\rangle_\tau - \langle C1, S2\rangle_\tau. \qquad (1b)$$

We then define the "correlation coherence":

$$\mathrm{coh}_\tau = (CO_\tau^2 + QD_\tau^2)^{1/2} \qquad (1c)$$

and the "correlation phase":

$$\mathrm{ph}_\tau = \tan^{-1}(-QD_\tau/CO_\tau). \qquad (1d)$$

This coherence is analogous to the usual correlation coefficient; the amount of linearly related variance at zonal wavenumber $k$ between positions $Z1$ and $Z2$ is proportional to this coherence squared. The phase is the actual longitude separation between the crests of zonal wavenumber $k$ at the two locations (only valid when the coherence is significant). Because the coherency statistic in time spectral analysis measures the correlation coefficient at each frequency (Jenkins and Watts, 1968, p. 353), these calculations are equivalent to time cross-spectral analysis integrated over all frequency bands. The methodology followed here is to construct maps of the coherence and phase in the meridional plane with respect to a particular reference position. Groups of these maps for different time lags then allows the evolving wave structure to be traced in time. Note that because these are correlation measurements, the relative coherence maxima/minima and rapid phase variations observed say nothing as to the standing or propagating nature of the oscillations; similar signatures would be observed in either case.

Confidence levels for the analyses presented here are discussed in appendix A. A simplified first order regressive model of the data suggests that cross-correlation coherence values on the order of 0.4 are necessary for confidence at the 95% level, although somewhat

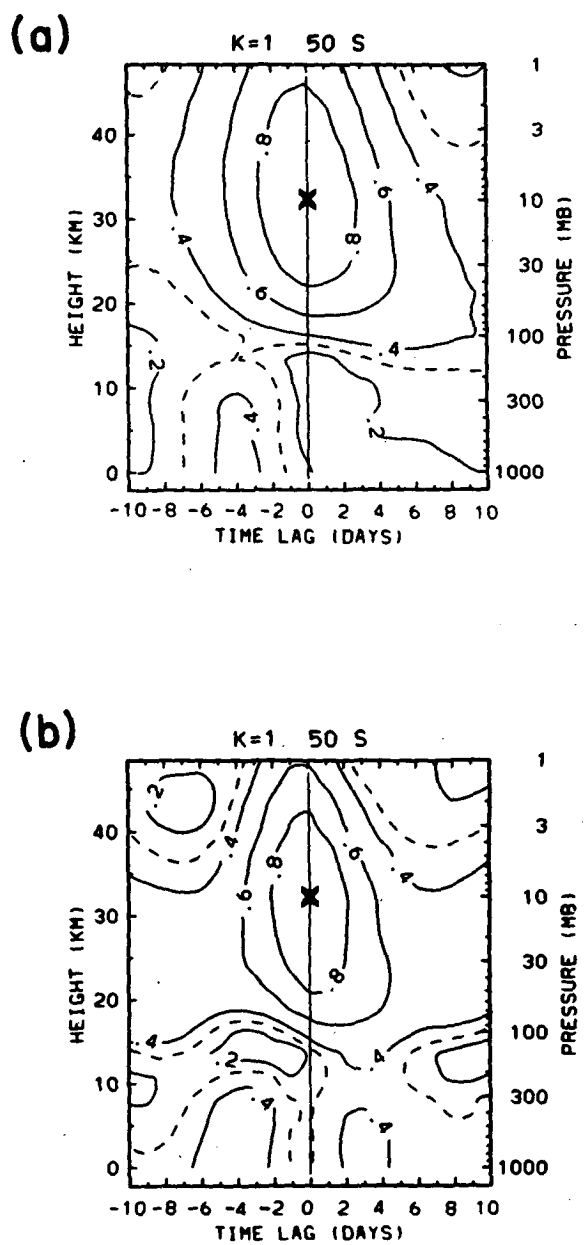


FIG. 5. (a) Vertical-time lag section at 50°S of the correlation coherence with respect to 10 mb, 50°S and zero time lag for wave 1 during the 1983 winter. Note the coherence maximum in the troposphere approximately 4 days preceding that at 10 mb. (b) As in (a) but for the 1984 winter.

larger values are necessary in the stratosphere for the wave 1 statistics (due to the strong autocorrelations there). Such a number is only a rough guide—the patterns observed here are evident over extended regions of latitude and height, and are delineated by slowly varying phase structures over "coherent" regions (and rapid phase variations in between). In addition, a high degree of reproducibility is found in the statistics over the two winters studied; several such examples will be exhibited.

Because these correlations are calculated over the full 120-day winter (June–September) studied here, no information on the seasonal dependence of wave propagation is available. The recent studies of Shiotani and Hirota (1985) and Mechoso et al. (1985) clearly show that wave activity is most vigorous in the SH stratosphere during late winter (August–September); this can be seen in the wave amplitude time series for 1983 shown in Fig. 3. This enhanced wave activity during late winter is probably a result of the downward and poleward evolution of the polar night jet, as discussed in Mechoso et al. (1985). The correlation statistics presented here are therefore somewhat biased towards being representative of later winter in the SH.

It should be noted, however, that clear episodes of vertical propagation are also observed during early winter (June–July) (see Fig. 13 of Part II and also Hartmann et al., 1984, and Mechoso et al., 1985). There appears to be some preference for the early winter events to be dominated by zonal wavenumber 1, whereas little other qualitative difference between early and late winter episodes is apparent. A detailed statistical analysis of the seasonality in wave propagation would require many years of data for stable estimates, and is beyond the scope of this paper.

## 3. Results—transient wave cross-correlation studies

Latitude–height contour plots of the correlation coherence and phase (Eq. 1) for particular zonal wavenumbers will be presented in this section. The coherence and phase are calculated with respect to a reference

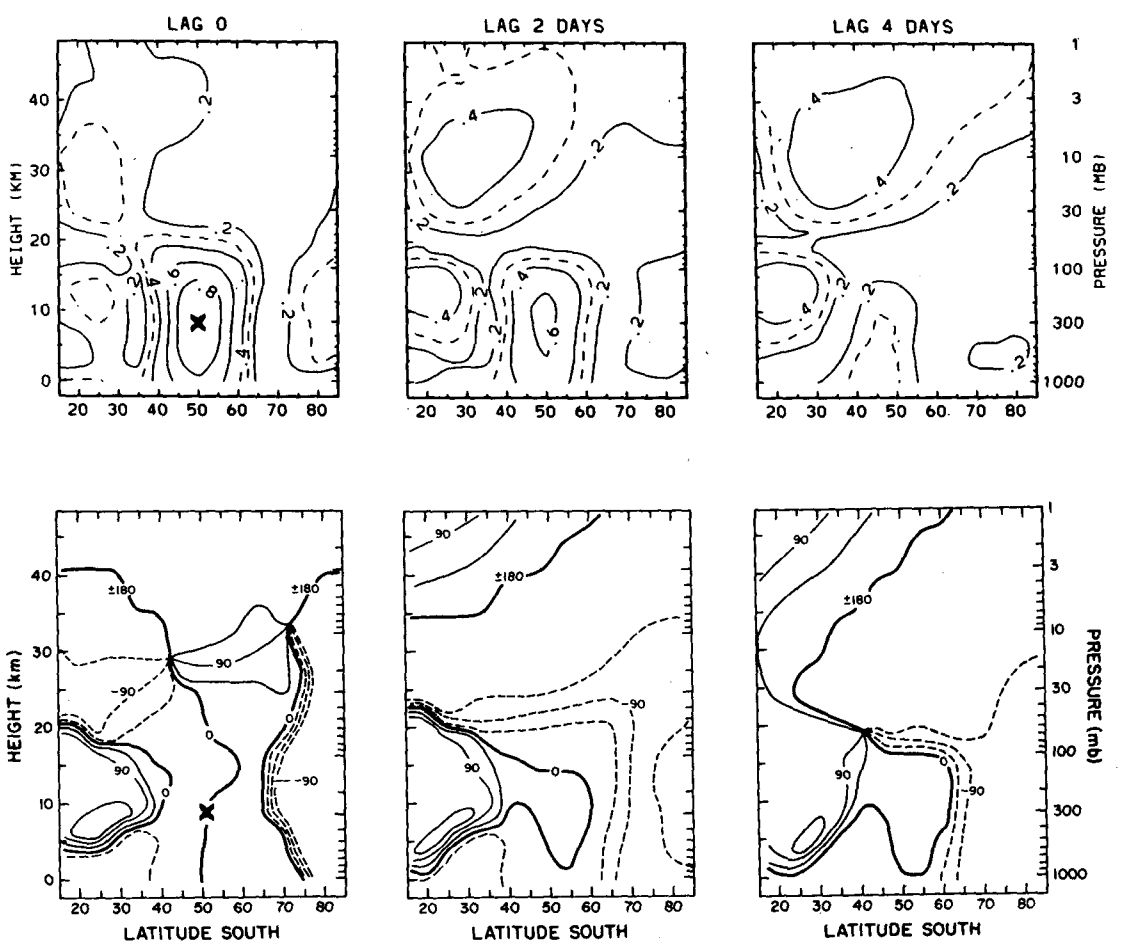


FIG. 6. As in Fig. 4, but for wave 1 cross-correlations with a reference at 300 mb, 50°S, for time lags of 0 (left), +2 (middle), and +4 days (right).

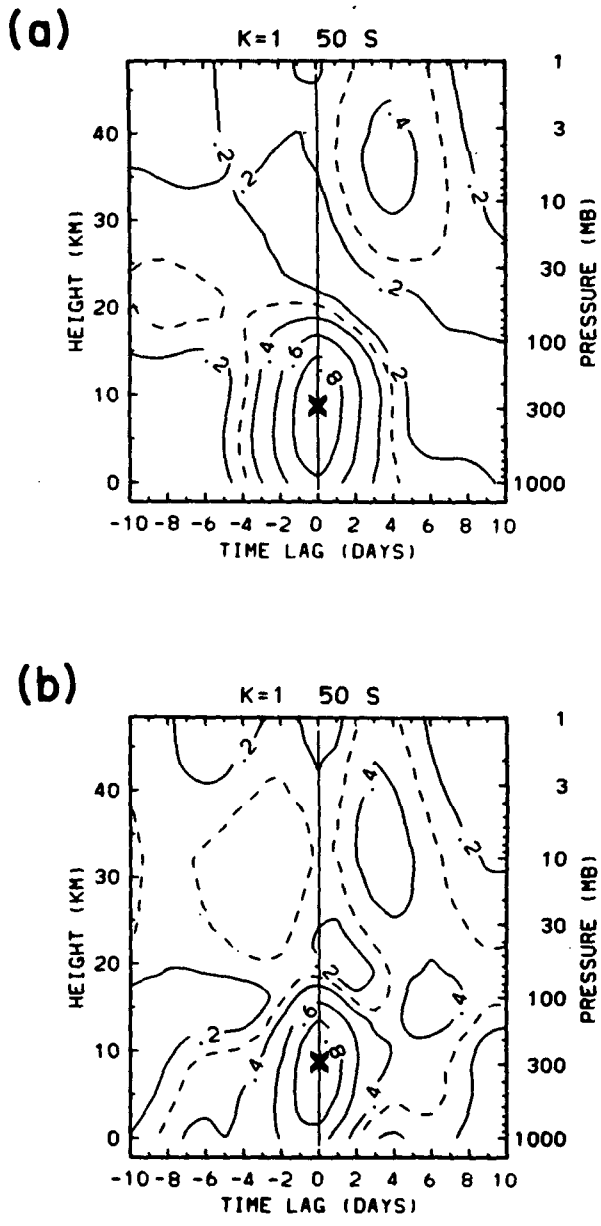


FIG. 7. (a) As in Fig. 5, but for wave 1 coherence with respect to 300 mb, 50°S for 1983. Panel (b) as in (a) but for 1984.

latitude/pressure (indicated by an 'X' in the figures) at zero time lag. The choice of the reference positions used will be discussed in section 4.

*a. k = 1*

Figure 4 shows the coherence and phase structures for wave 1 with respect to 50°S and 10 mb, for time lags of −4, −2 and 0 days. A single broad maxima of coherence is observed in the stratosphere, decreasing monotonically as the time lag is increased. Conversely, the coherence increases in the troposphere over 40°–55°S as the time lag is increased, showing that the stratospheric variance is linked to that in the troposphere several days earlier. A relative minimum in the coherence is observed between the tropospheric and stratospheric maxima, near 100 mb, and the phase structure shows a rapid 180° transition in this region. These pictures show that transient wave 1 fluctuations in the stratosphere are coupled to out of phase fluctuations in the midlatitude troposphere with a time lag indicative of upward propagation.

To delineate the time dependence more clearly, Fig. 5a displays a vertical section at 50°S of the coherence with respect to 10 mb, 50°S as a function of time lag. (The values at lags −4, −2 and 0 are the same coherence values at 50°S seen in Fig. 4). A clear maximum is observed in the troposphere centered near a lag of −4 days; this suggests a vertical propagation time scale for wave 1 between the troposphere and 10 mb level on

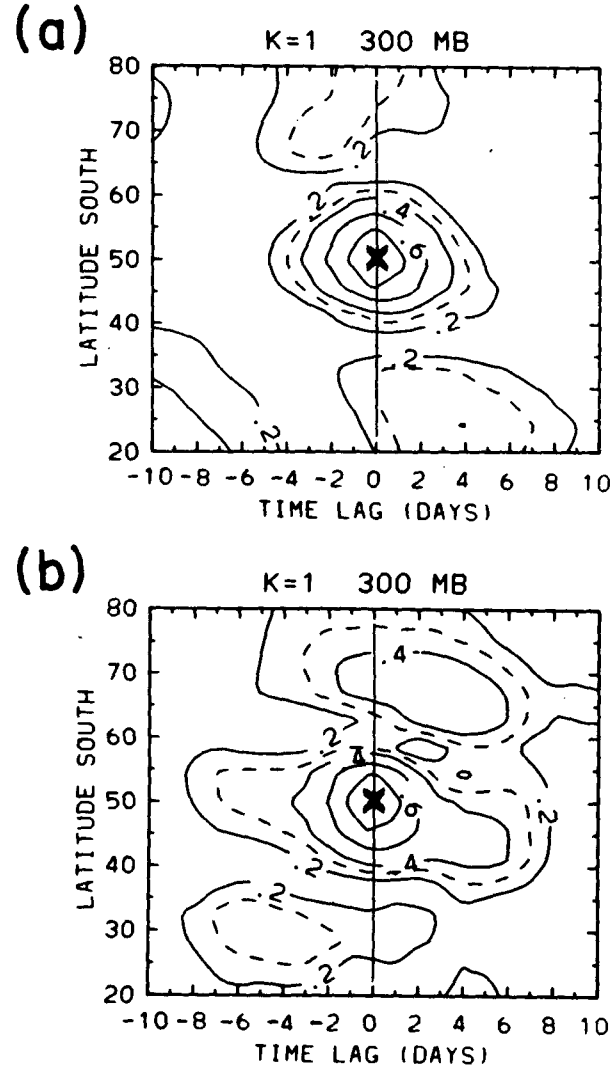


FIG. 8. (a) Latitude–time lag section at 300 mb of the correlation coherence with respect to 300 mb, 50°S and zero time lag for wave 1 during the 1983 winter. Note the clear 3-cell structure in latitude. (b) As in (a) but for 1984.

the order of 4 days. Figure 5b shows the same calculations for the 1984 winter season, and a remarkably similar time development is observed; a relative maximum in the troposphere 3–5 days prior to the 10 mb maximum, with small coherence between these two maxima coincident with a rapid 180° phase shift (not shown). Note that the stratospheric coherence maximum is found to descend slightly for positive time lags in both Figs. 5a–b, possibly indicating some downward wave movement after peak values at 10 mb—such behavior is also suggested by the EP flux signatures discussed in Part II. Also note that there is little evidence of upward propagation beyond the middle stratosphere in Figs. 5a, b.

Figure 6 shows the coherence and phase structures for wave 1, now with a reference position in the upper

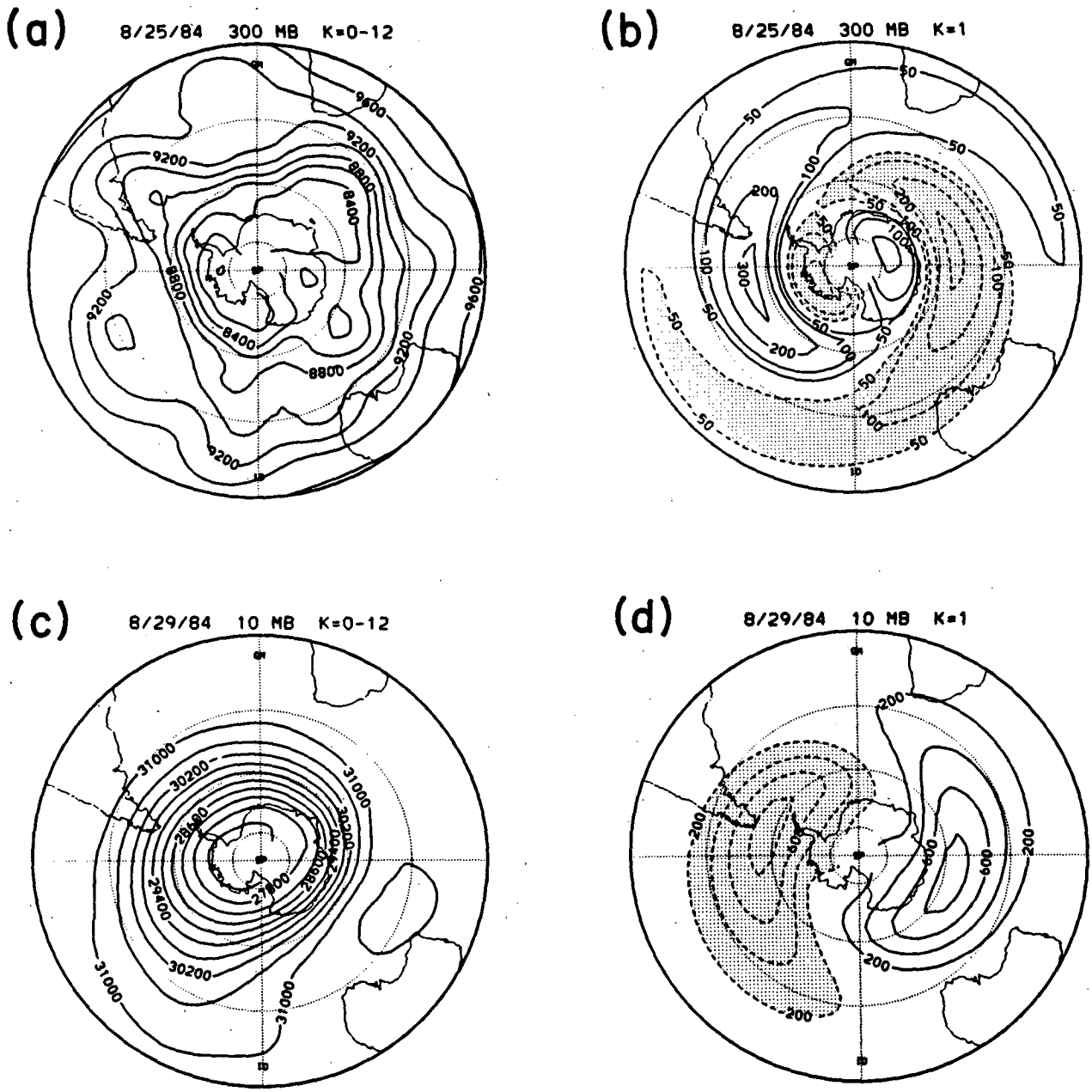


FIG. 9. (a) Polar stereographic projection of the 300 mb geopotential height contours on 25 August 1984, a time of large wave-1 amplitude in the troposphere. Contour interval 200 gpm. The outer latitude is 20°S. (b) As in (a) but the wave-1 component alone. Contour intervals of ±50, 100, 200, . . . gpm. Note the multiple maxima (minima) found along a meridian. (c) 10 mb wave 1 height field four days later, 29 August 1984. Contour interval of 200 gpm. Note the vertical out of phase character with the mid-latitude maximum in (b). (d) Total 10 mb height field on 29 August 1984. Contour interval of 400 gpm.

troposphere at 300 mb and 50°S, for time lags of 0, +2 and +4 days. Coherence with stratospheric levels is found to increase with the time lag. The poleward movement of the stratospheric coherence maximum seen in Fig. 6 is not observed during 1984; its significance is suspect. A relative minimum is observed between the stratospheric and tropospheric coherence maxima, coincident with rapid 180° phase variations. The altitude of the rapid vertical phase change is found near 10–30 mb at zero lag; as the coherence with the stratosphere grows in time, this region of rapid phase variation decreases in height to near 100 mb. Qualitatively similar behavior is found during 1984. This suggests that the vertical wavelength of wave 1 decreases somewhat after its initial excitation in the troposphere.

Figure 7a shows a vertical section at 50°S versus time lag (as in Fig. 5, now using a reference at 300 mb) to clarify these time variations—here a clear maximum is observed in the stratosphere for a time lag of +4 days. The strongest coherence in the stratosphere decreases with height above roughly 5 mb, again showing little evidence of upward propagation beyond the middle stratosphere. Similar characteristics are found for the 1984 winter in Fig. 7b. These calculations (with a reference in the troposphere) are complimentary to those of Figs. 4–5 (where the reference point was at 10 mb): both calculations isolate a vertical propagation time scale for wave 1 fluctuations on the order of four days.

Figure 6 also shows quite interesting meridional structure for wave 1 in the troposphere. As opposed to the single broad maximum in latitude observed in the stratosphere, three maxima in the coherence are observed in the troposphere (near 25°, 50° and 80°S). The two minima (near 35°S and 65°–70°S) coincide with rapid 180° phase variations—wave 1 thus exhibits a 3-cell structure in the troposphere with adjacent maxima out of phase by 180°. Note that the cross-correlations with the stratospheric reference position (Fig. 4) suggest that the tropospheric coherence maximum near 50°S is best correlated with the stratospheric variance.

Figure 8a displays a horizontal section at 300 mb of the time evolution of the coherence with respect to 300

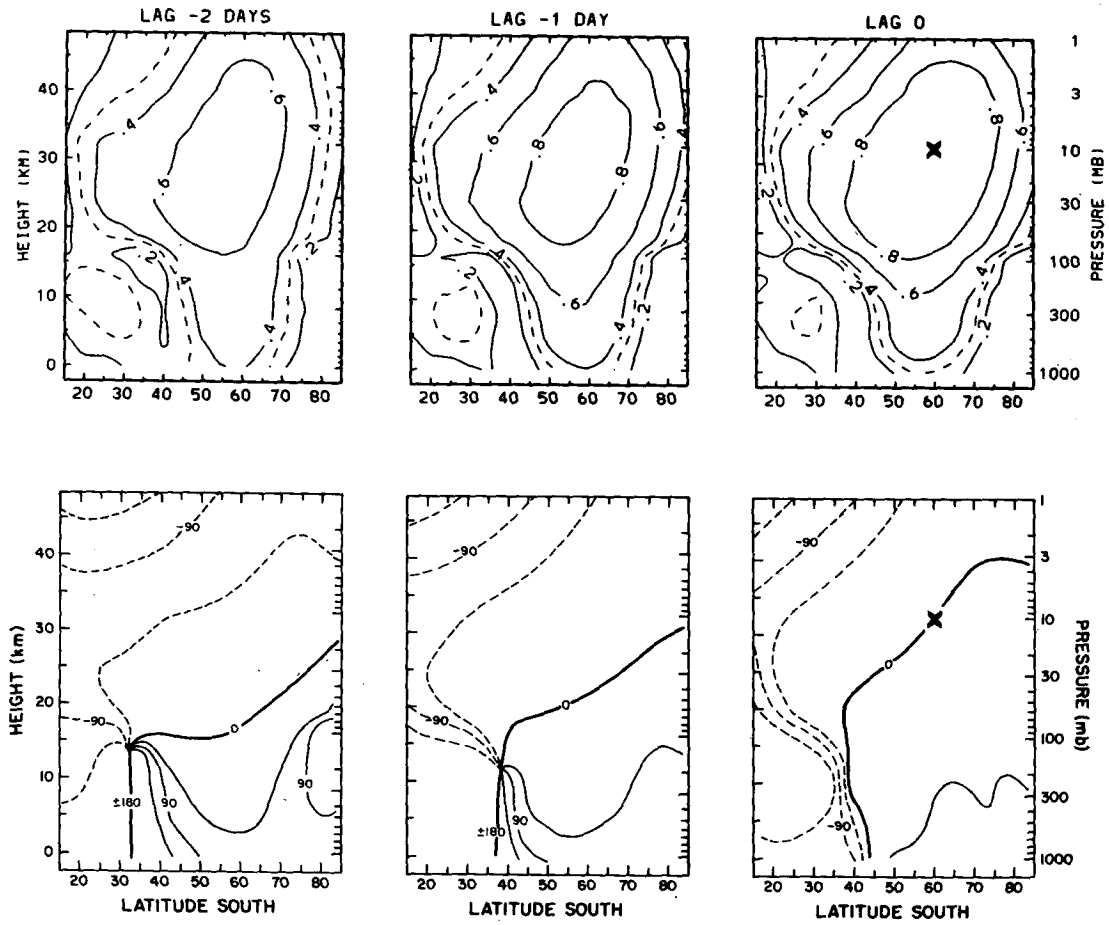


FIG. 10. As in Fig. 4 but for wave 2 cross-correlations with a reference at 10 mb, 60°S, for time lags of −2 (left), −1 (middle), and 0 days (right). The phases should be divided by two to give the actual longitudinal separation between crests.

mb and 50°S (values at 0, +2 and +4 days correspond to the 300 mb coherence values in Fig. 6). Here the three coherence maxima in latitude are clearly exhibited. Figure 8b shows similar calculations for the 1984 winter, and good consistency is again observed between the two winters. Note that although the relative positions of the maxima with respect to time in Fig. 8a is suggestive of equatorward group velocity, the orientation is reversed in Fig. 8b and the significance of any such association is suspect.

An example of the horizontal wave structure leading to such correlations is shown in Fig. 9 for a time when wave 1 amplitude is large. Figure 9a is the 300 mb geopotential height for 25 August 1984, while Fig. 9b displays the zonal wavenumber 1 component of this field alone. Three clear out-of-phase maxima can be traced along the 45°E meridian. The maximum (minimum) centered near 50°S has the shape of a drawn out tongue oriented NE–SW, such that it forms the maximum (minimum) in low latitudes on the opposite side of the globe. Figure 9c shows the 10 mb wave 1 geopotential four days later (29 August 1984), clearly illustrating the vertical out-of-phase behavior in mid-latitudes suggested by the correlation analysis. Note how the 10 mb structures are also arranged in tongues, although here the orientation is NW–SE, reversed from that at 300 mb. These latitudinal tilts are associated with meridional momentum flux: poleward in the stratosphere and equatorward in the troposphere. These momentum fluxes are clearly observed and discussed in Part II. Figure 9d is the total field at 10 mb, illustrating the asymmetry introduced by the strong wave 1.

*b. k = 2*

Figure 10 shows the coherence and phase structures for wave 2 with respect to 60°S and 10 mb, for time lags of 0, −1 and −2 days. The stratospheric maximum in coherence can be traced into the troposphere near 60°S, with slowly varying phase changes in the vertical (westward with height). Such vertical structure is distinct from that observed of the wave 1. The westward phase tilt with height at 60°S is largest for a time lag of −2 days. Because westward phase tilt with height is indicative of vertical propagation, the patterns in Fig. 10 are consistent with strong vertical propagation prior to upper level wave amplitude maxima.

Figures 11a, b display vertical sections at 60°S of the time development of the wave 2 coherence and phase with respect to 60°S and 10 mb. The coherence patterns (Fig. 11a) show strongest coherence with the troposphere for time lags of −1 to −2 days, approximately half the propagation time scale observed of the wave 1 statistics (Figs. 5a, b). The phase variations in time (with respect to the 10 mb level at lag 0) show regular eastward movement above the 100 mb level with a period near 13 days, in agreement with the quasi-regular eastward phase progression seen in Fig. 3. Note that zonal phase movement is not so (statistically) regular in the troposphere.

Figure 12 shows wave 2 coherence and phase cross sections with a reference position in the troposphere,

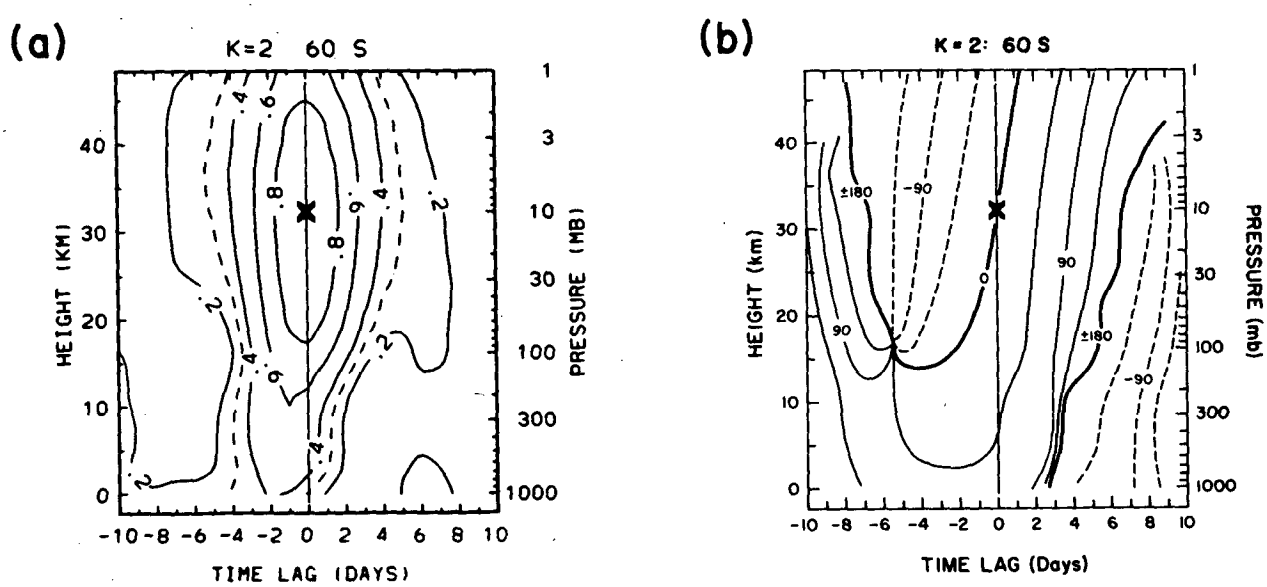


FIG. 11. (a) Vertical-time lag section at 60°S of the wave 2 coherence with respect to 10 mb and 60°S. Note maximum coherence in troposphere 1–2 days prior to that in the stratosphere. Panel (b) as in (a) but for wave 2 phase; divide by two to get the actual longitude separation between crests.

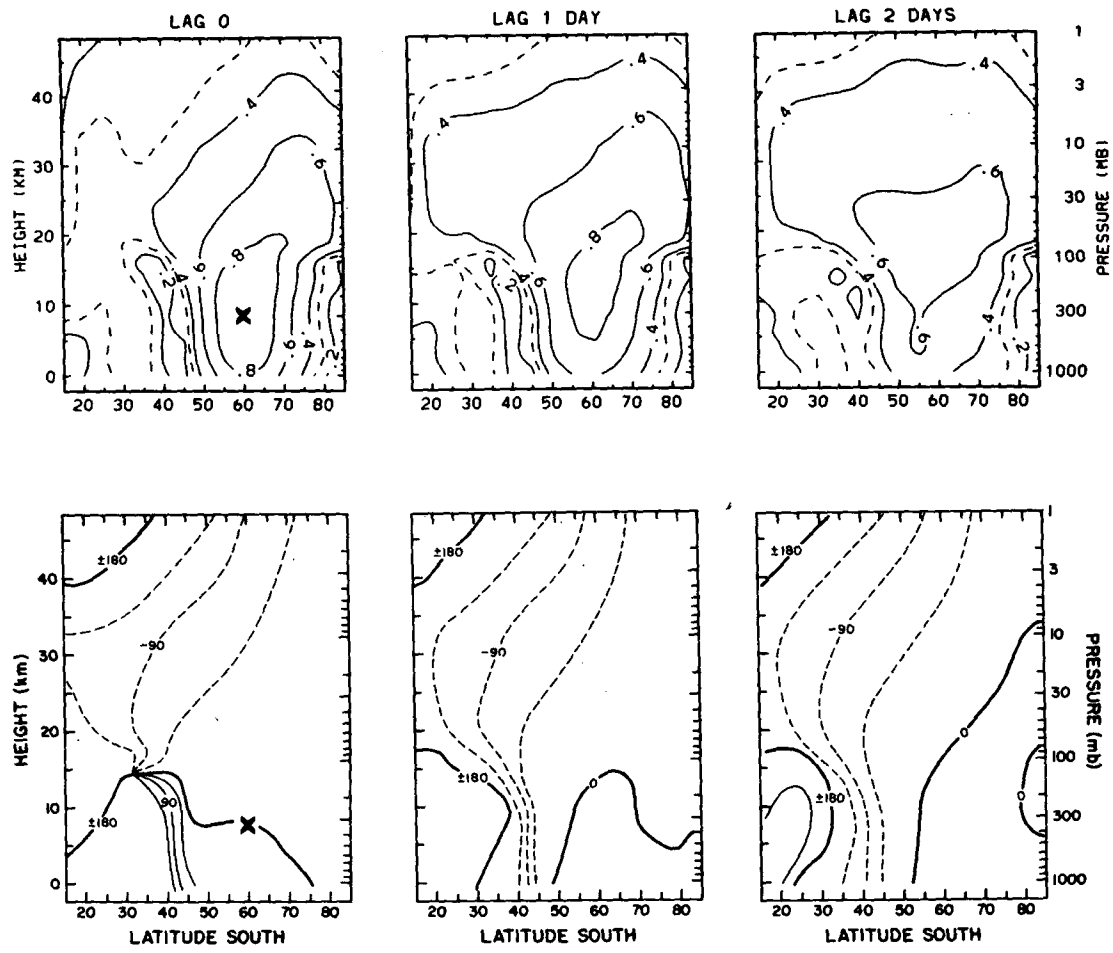


FIG. 12. As in Fig. 4, but for wave 2 cross-correlations with a reference at 300 mb, 60°S, for time lags of 0 (left), +1 (middle), and +2 days (right).

at 300 mb and 60°S. The strongest coherence levels at 60°S are seen to move upward as the time lag increases, clearly indicative of vertical propagation. This behavior is clarified in Fig. 13, which reiterates the vertical propagation time scale of 1–2 days. Note again, however, that little evidence of vertical propagation above the middle stratosphere is observed in either this figure or Fig. 11a.

The coherence and phase patterns in Fig. 12 show two out of phase latitudinal maxima in the troposphere for wave 2, centered near 60°S and 30°S, with a node near 40°S. A similar pattern can be seen in the tropospheric coherence and phase patterns associated with the 10 mb reference position in Fig. 10; it is also seen there that the stratospheric variance is most strongly related to the high latitude maximum near 60°S. This tropospheric structure is again distinct from the three-cell pattern in the troposphere found for wave 1.

Time-lag dependence of the coherence at 300 mb is shown in Fig. 14a, where the distinct high and low latitude maxima are clearly observed. Figure 14b is a similar plot for the 1984 winter; here the low latitude maximum exhibits a somewhat stronger coherence with 60°S than during 1983. The consistent patterns found here between the two winters again points to the fundamental nature of these correlations.

An example of a period of enhanced wave 2 activity throughout the troposphere and stratosphere is displayed in Fig. 15. Figure 15a shows the 300 mb geopotential height on 24 September 1983, while Fig. 15b shows the wave 2 contribution alone. Clear out of phase maxima are observed near 55°–60°S and 30°S; the low latitude maximum is of much smaller amplitude than that in high latitudes. Figure 15c displays the 10 mb wave 2 pattern one day later, 25 September 1983. A single broad maximum in latitude is observed in the stratosphere, shifted slightly westward with respect to the 300 mb pattern (Fig. 15b). Figure 15d is the total field at 10 mb, and the strong wave 2 signature is clearly seen.

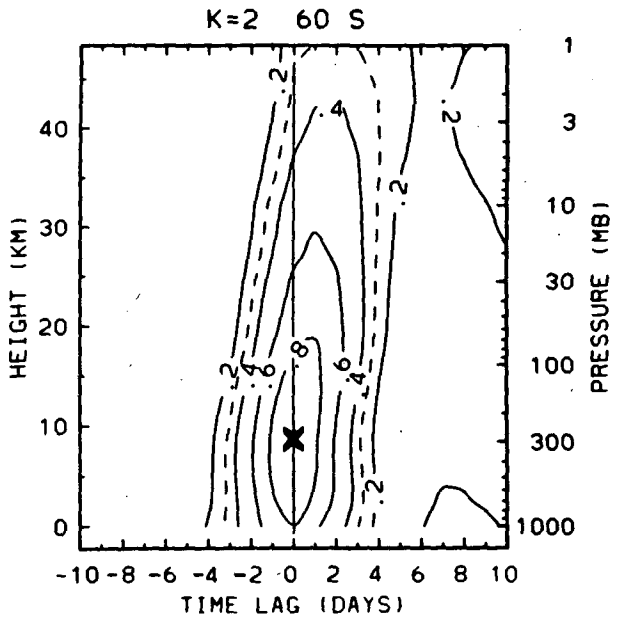


FIG. 13. As in Fig. 11a but with a reference position at 300 mb.

*c. k = 3*

The wave 3 cross-correlation patterns reveal an overall structure very similar to that observed for wave 2; because of this, they are discussed only briefly here. Figure 16a shows a vertical-time lag section at 55°S of the wave 3 coherence with respect to 55°S and 10 mb. The 10 mb variance is coherent with that in the troposphere, with a vertical propagation time scale on the order of one day (slightly faster than that for wave 2—see Fig. 11a). Figure 16b shows a similar plot, now with the reference position at 300 mb, and similar upward propagating behavior is seen. The phase variations in time (not shown) indicate eastward zonal progression in the stratosphere with a period near 7 days. Again no rapid phase shifts are observed in the vertical, only a westward tilt with height indicative of vertical propagation.

The wave 3 coherence and phase patterns reveal two out-of-phase maxima in latitude in the troposphere, similar to those observed for wave 2. Figure 17a shows a latitude–time lag section at 300 mb displaying this two cell structure for the 1983 winter, while Fig. 17b is a similar plot for 1984. Meridional cross sections (as in Fig. 10) clearly indicate that the stratospheric wave 3 variance is coherent and in phase with the high latitude tropospheric region near 55°S. For both winters (Figs. 17a, b) the maximum coherence at low latitudes precedes that at high latitudes, possibly suggestive of poleward wave group velocity, although the significance of such an association is certainly not strong.

*d. k = 4*

Figure 18 shows the coherence and phase of wave 4 at zero time lag for a reference of 300 mb and 50°S. A broad (in latitude) coherence maximum is found in the troposphere, with the hint of two out-of-phase coherent regions near 20°S and 80°S. The westward phase tilt with height (which is stronger for a time lag of −1 day) and NW–SE phase tilt in latitude (which is stronger for time lags of +1–2 days) are statistical signatures of baroclinic wave life cycles; this is also seen in the time average EP flux diagram for wave 4 (Fig. 1).

Time-development of the wave 4 coherence is seen in Fig. 19. Figure 19a is a vertical section at 50°S, showing little coherence between the troposphere and mid-to-upper stratosphere, although some hint of upward propagation is seen for a time lag of one day. The 300 mb latitude–time lag section (Fig. 19b) shows that the strongest low-latitude (20°S) coherence occurs after the midlatitude peak, consistent with the strong equa-

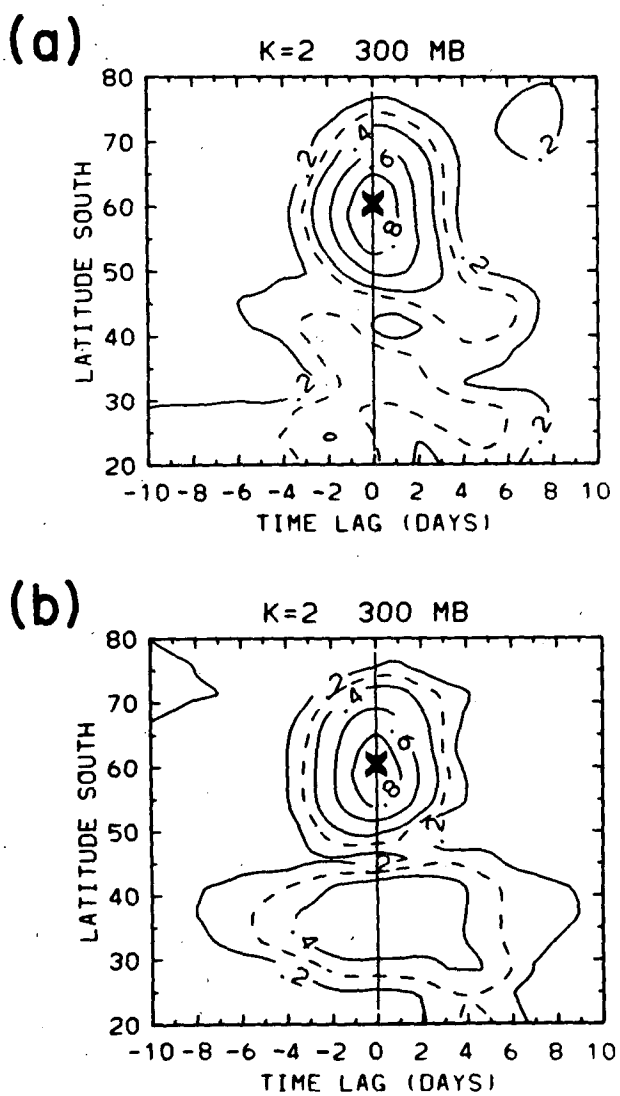


FIG. 14. As in Fig. 8 but for wave 2 coherence with respect to 60°S for (a) 1983, (b) 1984.

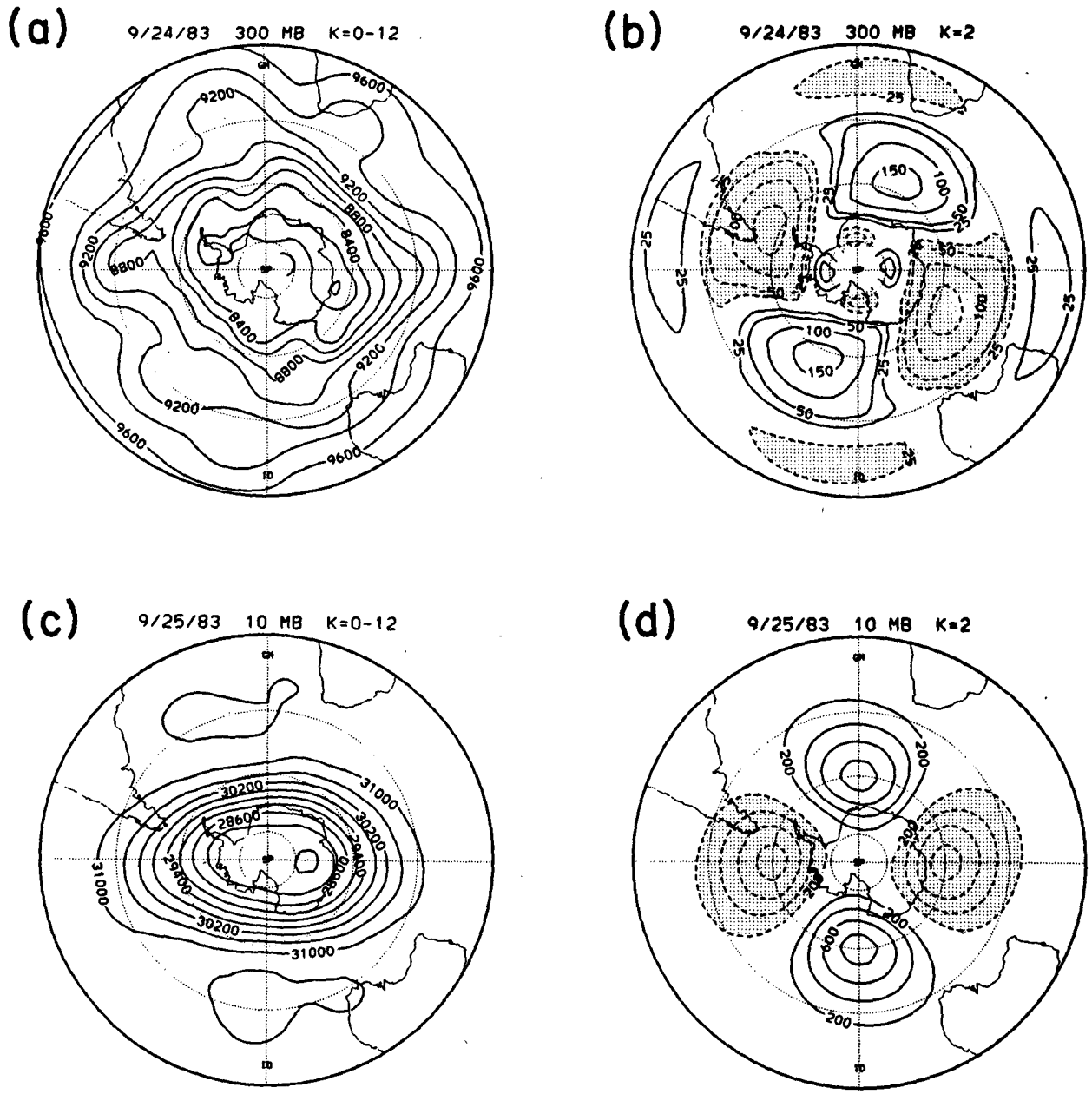


FIG. 15. As in Fig. 9 but for a period of enhanced wave 2 activity. (a) The 300 mb geopotential height for 24 September 1983. (b) As in (a) but for the wavenumber 2 component alone. Contour intervals of ±25, 50, 100, . . . gpm. (c) 10 mb $k = 2$ field on 25 September 1983. Contour interval of 200 gpm. (d) Total 10 mb field on 25 September 1983.

torward pointing EP flux (group velocity) vectors seen for wave 4 in Fig. 1.

## 4. Additional comments

### *a. Choice of reference positions*

The cross-correlation patterns obtained here are dependent on the particular reference positions chosen—note that different latitudes were chosen as tropospheric reference points for the $k = 1$ (50°S), $k = 2$ (60°S), and $k = 3$ (55°S) correlations. The choice of reference latitude can be made by considering cross-correlations with all latitudes, and simply choosing those reference points that show the strongest coherence with a 'distant' latitude (similar to determining 'teleconnectivity' maps). An objective way to determine positions of strong cross-correlation, taking into account information from all latitudes, is to perform a principal

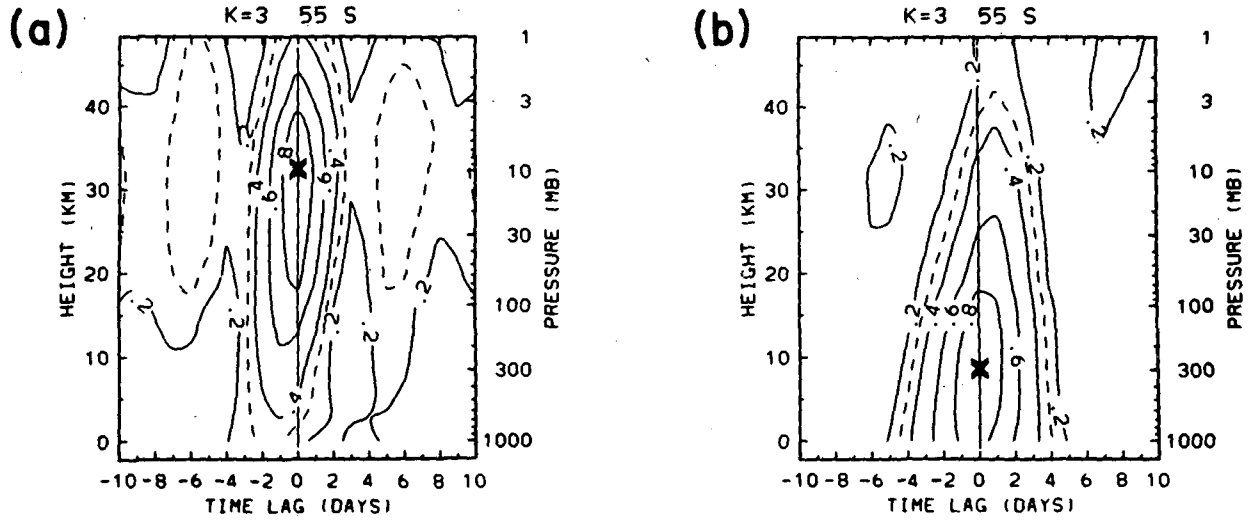


FIG. 16. (a) As in Fig. 5a but for wave 3 coherence at 55°S with respect to 55°S and 10 mb. (b) As in (a) but using a reference position at 300 mb. Both (a) and (b) show a one-day time lag between middle troposphere and middle stratosphere.

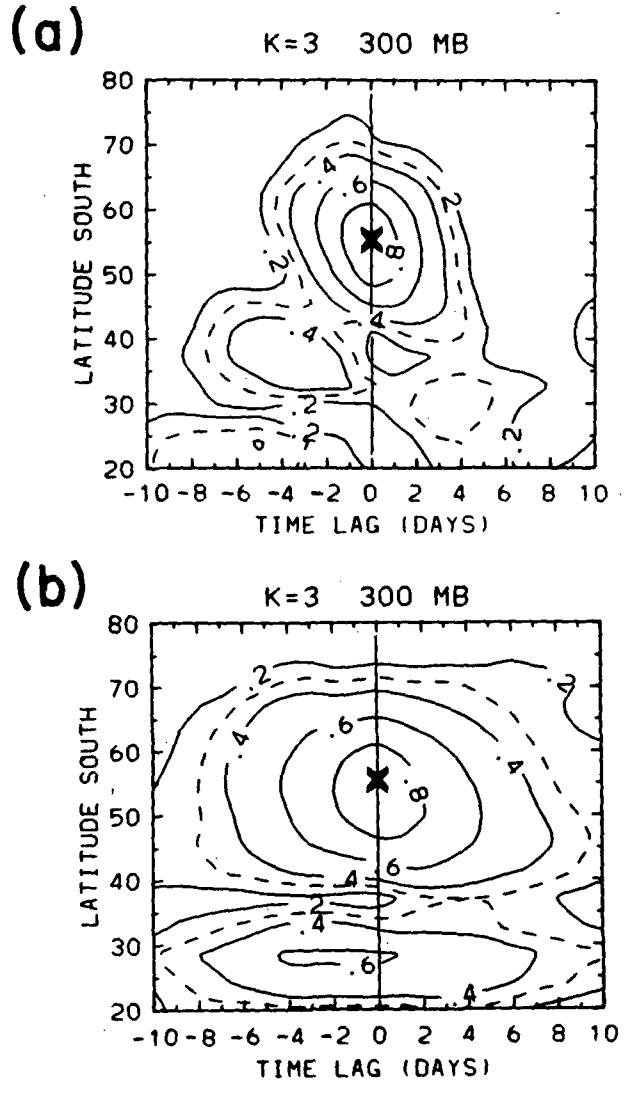


component analysis of cross-correlations from each possible reference latitude. If a single, dominant meridional structure is imbedded in the different cross-correlations, such an analysis will isolate it as contributing a majority of the variance.

To apply this method to the present situation, a cross-correlation (coherence) matrix is constructed using each successive latitude as reference, and the eigenvalues and eigenvectors are then calculated. For each wavenumber it was found that a single eigenstructure was dominant (contributing on the order of 60–70% of the overall variance). Figures 20a, b show the meridional structures associated with the dominant eigenvalues at 300 mb for waves 1 through 3, for both winters. Three relative maxima are found for wave 1, peaking near 25°, 50° and 75°S (much more robust during 1984). Because it was found that the stratospheric variance for wave 1 was most clearly linked to the troposphere near 50°S (see Fig. 4), this latitude was chosen as the tropospheric reference point.

The meridional eigenstructures for waves 2 and 3 both show clear double maxima in Fig. 20. Because the stratospheric variance was most clearly tied to the high latitude maximum for both waves (see Fig. 10), latitudes near the poleward maximum were used as references (60°S for $k = 2$ and 55°S for $k = 3$). Note that the positions of the maxima (and minima) are different between the two winters (compare especially the $k = 2$ patterns), suggesting that the absolute latitude positions are not as fundamental as the number of maxima (minima) for each zonal wavenumber. A similar analysis at stratospheric levels reveals single broad maxima for each wavenumber; the coherence patterns

FIG. 17. As in Fig. 8 but for wave 3 coherence at 300 mb with respect to 55°S, for (a) 1983, (b) 1984.

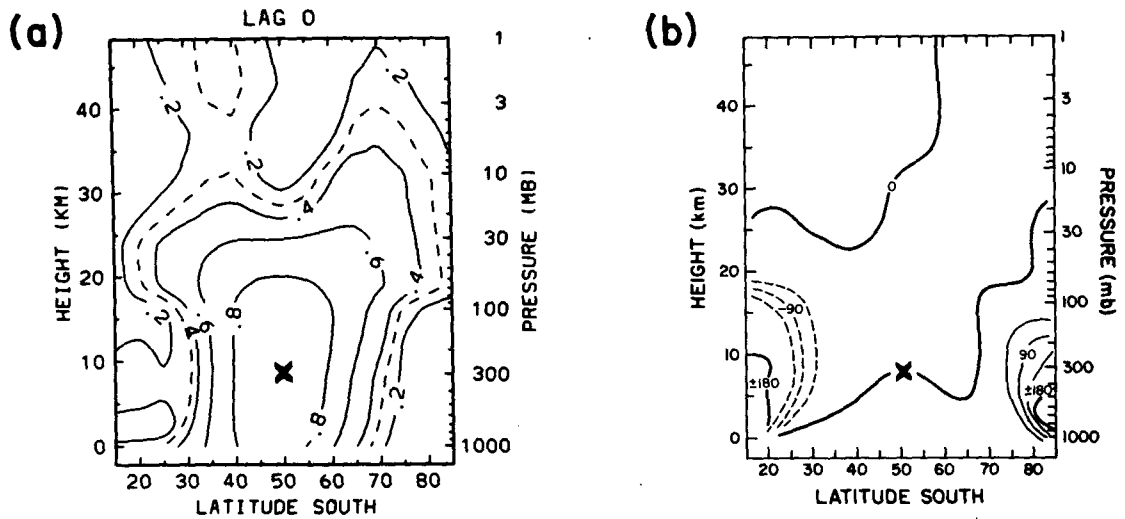


FIG. 18. Meridional sections of the correlation coherence (a) and phase (b) for wave 4 with respect to 50°S and 300 mb at zero time lag.

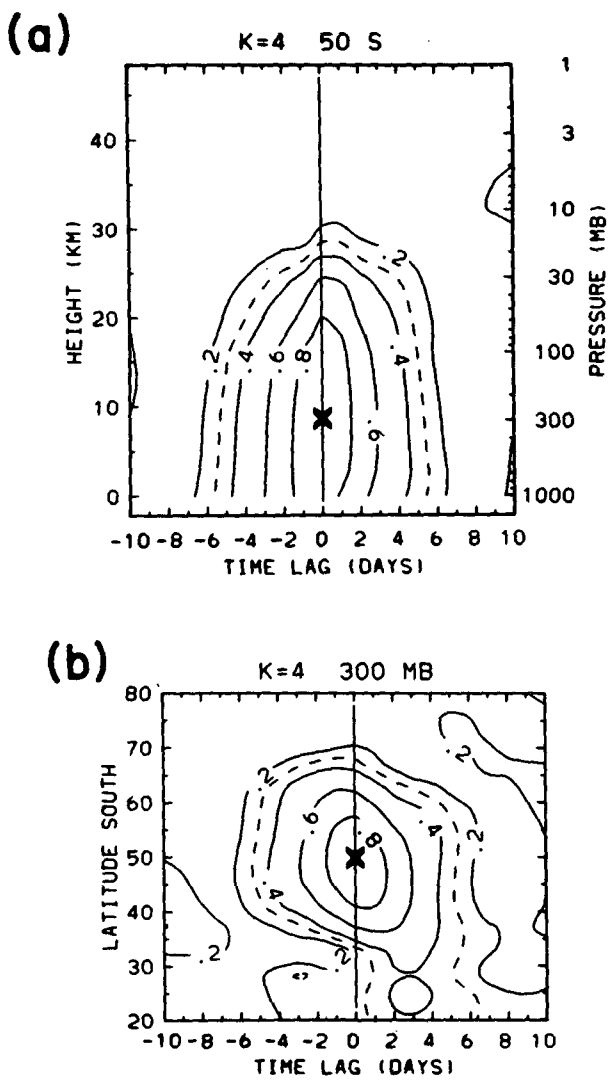


are more or less independent of reference position. The stratospheric reference latitudes were chosen to match those in the troposphere.

*b. Time spectral analysis*

Because the analysis technique employed here inherently measures the coherence integrated over all frequencies, a natural extension is to inquire as to the time spectral dependence of the observed cross-correlations. In addition to determining the time scales relevant to the observed coherent fluctuations, such an analysis might also allow detection of coherent signal(s) not seen in the integrated analysis.

An example of such a calculation is illustrated in Fig. 21, where a meridional cross-section of the wave 1 coherence with respect to 50°S and 300 mb (at zero time lag) is shown at left for the 1984 winter (compare with the similar calculation for 1983, shown in the top left panel of Fig. 6—note the clear 3-cell structure in the troposphere). For this example, the time spectral dependence of the coherence between 50°S, 300 mb and 70°S, 300 mb is investigated—the correlation coherence value is 0.47. The middle of Fig. 21 displays the power spectra of the wave 1 fluctuations at each position, and the right-hand plots show the coherence and phase between these positions as functions of frequency. These spectral estimates were calculated by direct Fourier transform, and smoothed by averaging over five adjacent frequency bands. The power spectra at both latitudes show a quite red behavior, with most of the power concentrated at periods longer than 10 days (corresponding to the episodic wave amplitude

FIG. 19. (a) As in Fig. 5a but for wave 4 coherence at 50°S with respect to 300 mb and 50°S. (b) as in Fig. 8a but for wave 4 coherence at 300 mb with respect to 300 mb and 50°S.

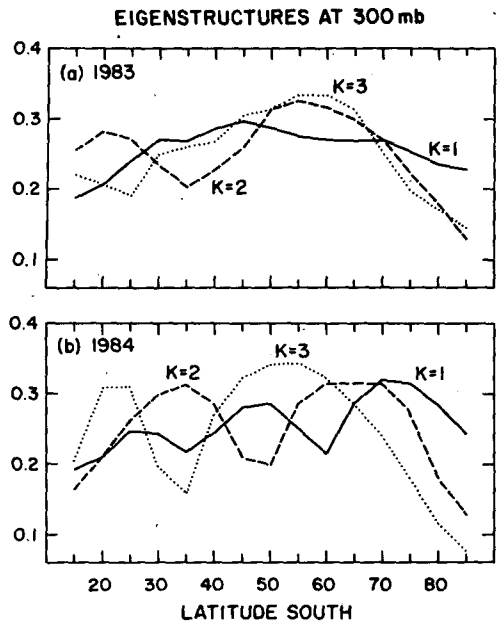


FIG. 20. Predominant eigenstructures resulting from the EOF analysis at 300 mb of correlation coherences using each latitude (15–85°S) as reference position, for (a) 1983 and (b) 1984. Note the three maxima for wave 1 and two maxima for waves 2 and 3. These calculations were the basis for the choices of reference latitudes used in the correlation analyses.

fluctuations, as in Fig. 3). The coherence is a maximum at the lowest frequencies (where most of the power is), and is significantly above the integrated value of 0.47. Note also that the phase difference is close to 180° for the lowest frequency spectral estimates (the integrated value is 172°), whereas it is more variable over the rest of the spectrum.

Those calculations show that the observed coherent, out-of-phase behavior exhibited between these latitudes is clearly related to the low frequency amplitude fluctuations (wave growth episodes) the waves are observed to undergo. Similar behavior is observed of the coherent stratosphere–troposphere fluctuations, and likewise the wave 2 and wave 3 statistics.

## 5. Discussion

The statistical correlations observed of the planetary waves in this study is summarized schematically in Fig. 22. Here regions in the meridional plane that exhibit enhanced coherence with other "distant" regions are demarked with heavy dashed lines. As denoted by the clear and dashed coherence maxima, the fluctuations are out of phase between adjacent coherent regions in the troposphere, as well as between the stratosphere and midlatitude troposphere for wave 1. Additionally, the strongest stratosphere–troposphere cross-coherence is indicated with the arrows for each wavenumber in

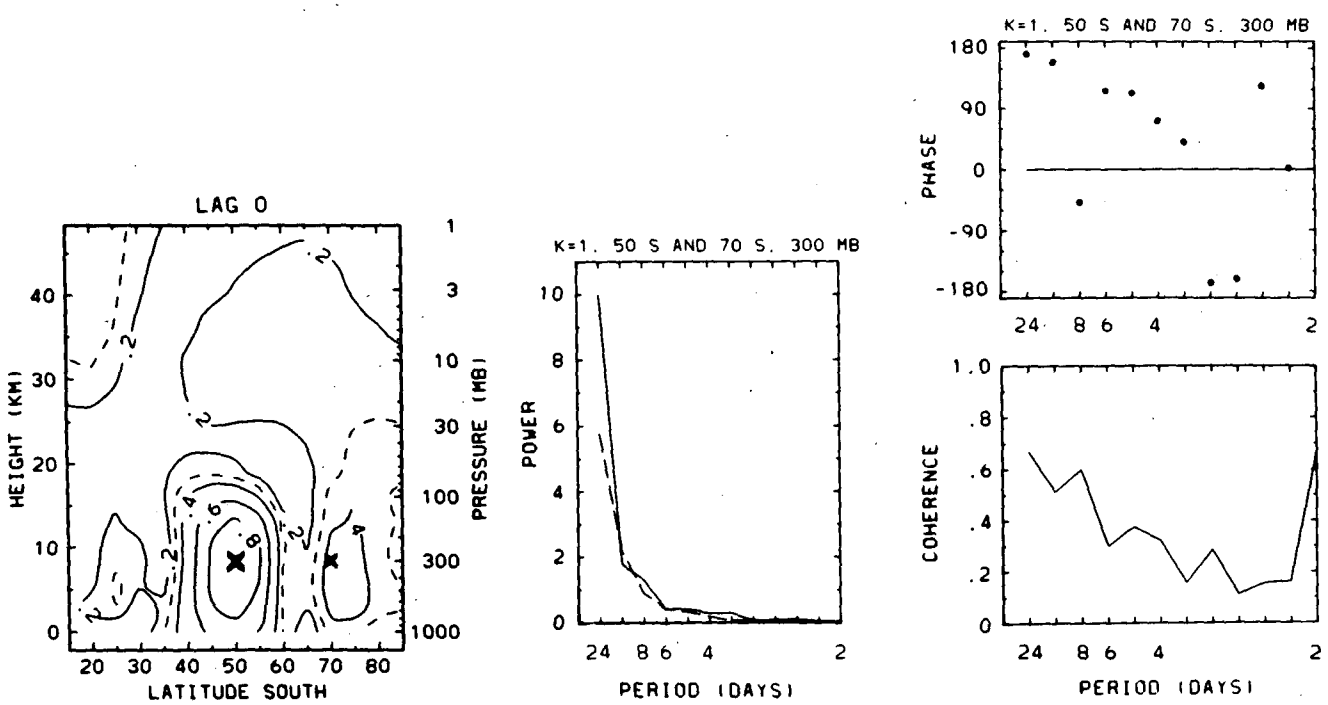


FIG. 21. Left: Meridional section of the wave 1 coherence at zero time lag with respect to 50°S and 300 mb for the 1984 winter. The correlation coherence between 50°S, 300 mb and 70°S, 300 mb is 0.47; the relative phase difference (not shown) is 172°. Middle: One-sided power spectra for 50°S, 300 mb (solid) and 70°S, 300 mb (dashed), normalized to a maximum value of 10. Right: Phase in degrees (upper) and coherence (lower) between these two positions as functions of period.

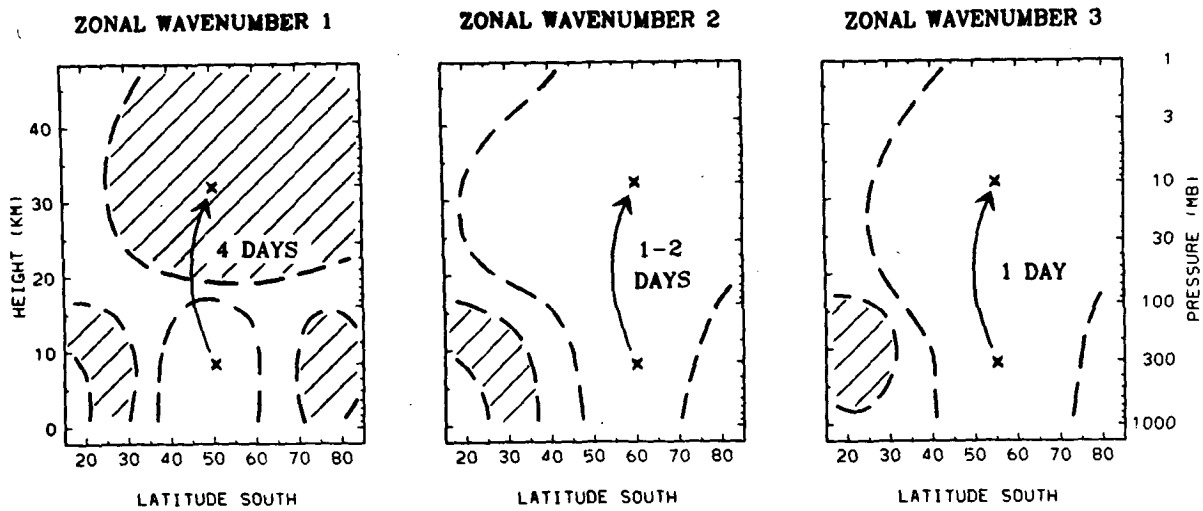


FIG. 22. Schematic diagram of planetary wave structure and propagation observed in this study. See text for details.

Fig. 22, along with the observed time lag in each case. We associate these observed time lags with the time scales for vertical propagation between the middle troposphere and middle stratosphere for each wavenumber.

As hypothesized by Mechoso and Hartmann (1982), the lack of coherence they observed between troposphere and stratosphere is a result of the finite time it takes for the waves to propagate vertically. The cross-correlation analysis used here allows such time lag information to be deduced. Clear vertical group velocity dispersion is observed between waves 1–3, with wave 1 taking several days longer than waves 2 and 3 to move upwards (and wave 2 taking longer than wave 3). Such vertical dispersion was observed in the theoretical ray-tracing calculations of Karoly and Hoskins (1982), based upon idealized NH winter basic states. They also observed vertical propagation time scales on the same order as those observed here.

The vertical structure of wave 1 differs fundamentally from that of waves 2 and 3, with an out of phase relationship observed between the strongest coherent regions in the troposphere and stratosphere. Three out-of-phase maxima are found in the troposphere; the middle latitude maximum (near 50°S) is most coherent with the stratospheric variance. Waves 2 and 3 exhibit coherence profiles in the meridional plane very similar to each other, with out-of-phase high and low latitude tropospheric maxima, and in phase variations between the stratosphere and the high latitude tropospheric maxima. Westward phase tilts with height are strong prior to stratospheric amplitude maxima; this behavior, which is consistent with vertical energy propagation, is discussed more fully and quantified in Part II.

The fundamental difference in vertical structure between wave 1 fluctuations and those of shorter zonal scale suggests that a zonal wavenumber breakdown may be physically meaningful here. This is a surprising finding in light of the very similar energetic characteristics exhibited by waves 1 and 2 (discussed in Part II), and the fact that planetary wave excitation in the troposphere usually has spectral components of both wave 1 and wave 2, which then disperse vertically as observed in this study. Some light might be shed on this question by examining the horizontal structure of the in-phase versus out-of-phase variations between 10 and 300 mb, thus avoiding the biases of prior zonal wavenumber decomposition. Along these same lines, examination of the vertical coherence/phase structure of analyses based on two-dimensional wavenumber (spherical harmonic decomposition) would provide additional insight into the horizontal character of these fluctuations. It will also be of interest to examine NH statistics in a manner similar to that used here to see if similar coherent variations are evident.

Discussion of the planetary wave forcing mechanisms and their relation to the observed wave structure is deferred to the discussion section of Part II.

## APPENDIX A

### Confidence Levels

To establish confidence levels for the cross-correlations discussed here, the analysis of Lau and Chan (1983) is followed. Based on the assumption that the data can be modeled as first order regressive processes, they derive a formula for the standard deviation of the cross-correlation coefficient $\langle A, B\rangle_\tau$ between time series A and B (at time lag $\tau$):

$$SD(r(\tau)) = \left[\frac{2}{(N-|\tau|)[1-\exp(-(\lambda_A+\lambda_B))]}\right]^{1/2} \quad \text{(A1)}$$

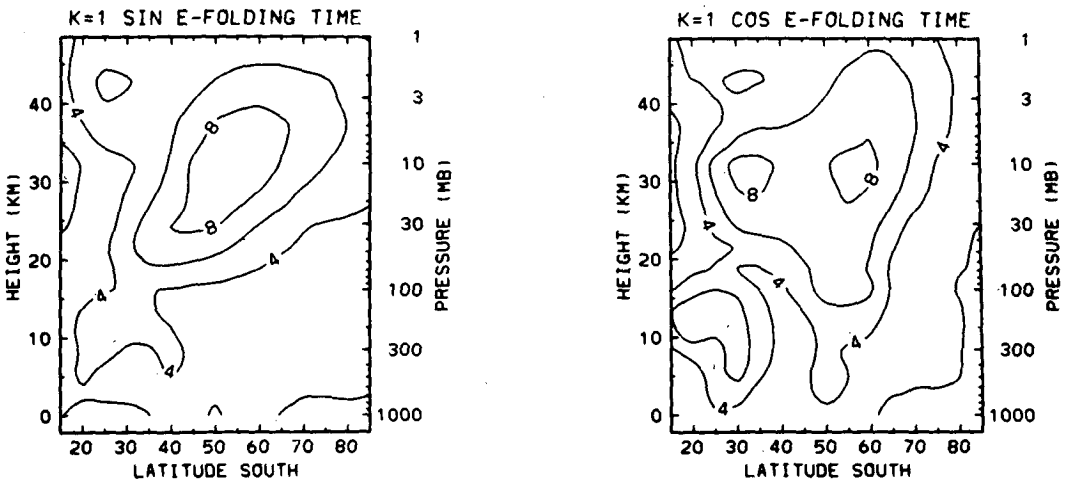


FIG. A1. Meridional cross sections of the *e*-folding time scales (in days) for wave 1 sine (left) and cosine (right) time series during 1983, estimated by fitting the observed autocorrelation curves to a first order regressive process (described in Appendix). Note the relatively long time scales in the stratosphere.

where $N$ is the length of the time series, and $\lambda_A(\lambda_B)$ is the inverse autocorrelation *e*-folding time of series A(B).

Autocorrelation *e*-folding times are estimated here by fitting the observed lagged autocorrelations up to a lag of 10 days to a first order regressive process with a least squares fit. Although the observed lagged autocorrelations are not strictly first-order regressive, it is not a bad first approximation, and this method allows for an objective estimation procedure. Figure A1 shows meridional cross-sections of the autocorrelation *e*-folding time scales for wave 1 sine and cosine time series during 1983. The most distinctive feature seen here is the relatively long time scales in the stratosphere (of order 8 days) versus shorter time scales (of order 2–3 days) in the troposphere. We speculate that the short time scales observed for wave 1 in the troposphere are linked to interactions with the shorter, baroclinically forced waves, which we find to also exhibit time scales on the order of 2–3 days. Planetary waves in the stratosphere are free from such dominating effects.

We find that the sine and cosine time series for all other wavenumbers exhibit time scales on the order of 2–3 days throughout 1000–1 mb. Note that for a disturbance which is regularly propagating in the zonal direction, the sine and cosine series are harmonic in time, and the autocorrelations fall to a value of $1/e$ in approximately 0.2 times the wave period. This sets a limit on the wave 2 sine and cosine time scales in the stratosphere on the order of 2 days (given the observed zonal period of $\approx$13 days). Although not directly important here, we note that the wave 2 *amplitude* time series (which is not necessarily tied to its period) exhibits longer time scales in the stratosphere (of order 4 days) than in the troposphere (2–3 days).

The longer autocorrelation *e*-folding time scales observed in the stratosphere in Fig. A1 mandate that larger wave 1 cross-correlation values are necessary for significance. Table A1 shows what cross-correlation values are necessary for confidence at the 95% level (calculated from Eq. A1) given various values of the *e*-folding time. For wave 1 cross-correlations between midlatitude stratospheric levels, a value ~0.5–0.6 is necessary; between midlatitude stratosphere and troposphere ~0.4–0.5, and between tropospheric levels ~0.4. Because higher wavenumbers show shorter autocorrelation times, cross-correlations near 0.4 are necessary.

TABLE A1. The 95% confidence level for cross-correlation between time series A and B with the given *e*-folding time scales $\lambda_A^{-1}$ and $\lambda_B^{-1}$ (from Eq. A1, with $(N - |\tau|) = 110$ days).

| $\lambda_A^{-1}$ (days) | $\lambda_B^{-1}$ (days) | 95% confidence level |
|---|---|---|
| 2 | 2 | 0.34 |
| 3 | 3 | 0.39 |
| 3 | 6 | 0.43 |
| 3 | 9 | 0.45 |
| 6 | 6 | 0.51 |
| 6 | 9 | 0.55 |
| 9 | 9 | 0.60 |

*Acknowledgments.* The author thanks Chuck Graves for his assistance in development of the cross-spectral correlation analysis.

## REFERENCES

Edmon, H. J., B. J. Hoskins and M. E. McIntyre, 1980: Eliassen-Palm cross sections for the troposphere. *J. Atmos. Sci.*, **37**, 2600–2616. See also Corrigendum, **38**, 1115.

Hartmann, D. L., 1976: The structure of the stratosphere in the

Southern Hemisphere during late winter 1973 as observed by satellite. *J. Atmos. Sci.*, **33**, 1141–1154.

——, C. R. Mechoso and K. Yamazaki, 1984: Observations of wave–mean flow interaction in the Southern Hemisphere. *J. Atmos. Sci.*, **41**, 351–361.

Harwood, R. S., 1975: The temperature structure of the Southern Hemisphere stratosphere August–October 1971. *Quart. J. Roy. Met. Soc.*, **101**, 75–91.

Hirota, I., and Y. Sato, 1969: Periodic variation of the winter circulation and intermittent vertical propagation of planetary waves. *J. Meteor. Soc. Japan*, **47**, 390–402.

Jenkins, G. E., and D. G. Watts, 1968: *Spectral Analysis and its Applications*, Holden-Day, 525 pp.

Karoly, D. J., and B. J. Hoskins, 1982: Three-dimensional propagation of planetary waves. *J. Meteor. Soc. Japan*, **60**, 109–122.

Lau, K.-M., and P. H. Chan, 1983: Short-term climate variability and atmospheric teleconnections from satellite-observed outgoing longwave radiation. Part II: Lagged correlations. *J. Atmos. Sci.*, **40**, 2751–2767.

Leovy, C. B., and P. J. Webster, 1976: Stratospheric long waves: Comparison of thermal structure in the Northern and Southern Hemispheres. *J. Atmos. Sci.*, **33**, 1624–1638.

Mechoso, C. R., and D. L. Hartmann, 1982: An observational study of traveling planetary waves in the Southern Hemisphere. *J. Atmos. Sci.*, **39**, 1921–1935.

——, —— and J. D. Farrara, 1985: Climatology and interannual variability of wave, mean-flow interaction in the Southern Hemisphere. *J. Atmos. Sci.*, **42**, 2189–2206.

Muench, H. S., 1965: On the dynamics of the winter stratospheric circulation. *J. Atmos. Sci.*, **22**, 349–360.

O'Neill, A., and B. F. Taylor, 1979: A study of the major stratospheric warming of 1976/77. *Quart. J. Roy. Meteor. Soc.*, **105**, 71–92.

Quiroz, R. S., 1979: Tropospheric–stratospheric interaction in the major warming event of January–February 1979. *Geophys. Res. Lett.*, **6**, 645–648.

Randel, W. J., and J. L. Stanford, 1985: The observed life cycle of a baroclinic instability. *J. Atmos. Sci.*, **42**, 1172–1188.

——, D. E. Stevens and J. L. Stanford, 1987: A study of planetary waves in the southern winter troposphere and stratosphere. Part II: Life-cycles. *J. Atmos. Sci.*, **44**, 936–949.

Shiotani, M., and I. Hirota, 1985: Planetary wave-mean flow interaction in the stratosphere: a comparison between Northern and Southern Hemispheres. *Quart. J. Roy. Met. Soc.*, **111**, 309–334.

van Loon, H., and R. L. Jenne, 1972: The zonal harmonic standing waves in the Southern Hemisphere. *J. Geophys. Res.*, **77**, 3846–3855.